Polym. Korea, Vol. 50, No. 5, pp. 671-686 (2026)
https://doi.org/10.7317/pk.2026.50.5.671
ISSN 2234-8077(Online)

COOH 관능화 그래핀 나노플레이트렛 함량이 천연고무/브로모부틸고무 블렌드의 물성에 미치는 영향

K. Senthilvel, S. Vishnu*, and B. Prabu*,†
Department of Mechanical Engineering, Karaikal Polytechnic College
*Department of Mechanical Engineering, Puducherry Technological University
(2026년 1월 5일 접수, 2026년 8월 7일 수정, 2026년 8월 7일 채택)

Characterization and Properties of COOH Functionalized Graphene Nanoplatelets Filled Natural Rubber/Bromo-Butyl Rubber Blends

K. Senthilvel, S. Vishnu*, and B. Prabu*,†
Department of Mechanical Engineering, Karaikal Polytechnic College, Karaikal, Puducherry, India
**Department of Mechanical Engineering, Puducherry Technological University, Puducherry, India*
(Received January 5, 2026; Revised August 7, 2026; Accepted August 7, 2026)

Abstract: Natural rubber–bromobutyl rubber (NR–BIIR) composites containing 0–9 phr COOH-functionalized graphene nanoplatelets (FGNP) were prepared by melt blending using a two-roll open mill. FGNP dispersion and interfacial interactions within the NR–BIIR matrix were examined by field-emission scanning electron microscopy (FESEM) and X-ray diffraction (XRD). The composites exhibited significant enhancements in mechanical, thermal, and dynamic mechanical properties compared to NR–BIIR gum. At 5 phr FGNP loading, improvements of 22.9, 19, 32.6, 30.2, and 24% were observed in stress at rupture, elongation at failure, modulus at 100% strain, tear resistance and abrasion loss respectively. These improvements are attributed to uniform FGNP dispersion, as confirmed by FESEM and XRD. Enhanced interfacial adhesion was evidenced by increased storage modulus (E') and glass transition temperature (T_g). Thermogravimetric analysis showed that the T_{10}, T_{50} and char residue at 600 °C of 5 phr FGNP-reinforced composites were 2.5, 3.2 °C and 102% higher than NR–BIIR gum.

Keywords: natural rubber-bromobutyl rubber blends, functionalized graphene nanoplatelets, mechanical attributes, thermal stability, viscoelastic behaviour.

Introduction

Academics and business have paid a lot of interest to graphene, a revolutionary one-atom-thick carbon material that is structured in a hexagonal honeycomb lattice.[1] Due to its substantial theoretical specific surface area, high Young's modulus, and exceptional electrical and thermal conductivities, graphene has emerged as a promising filler for rubber composites.[2-4] Nonetheless, the commercial scale-up of few-layer graphene and its enormous costs are impeding its extensive use. Consequently, graphene oxide, reduced graphene oxide, and graphene nanoplatelets have intrigued considerable passion as a cost-effective and feasible alternative to graphene in large-scale applications.

Graphene nanoplatelets (GNPs) are platelet-liked graphite nanocrystals consisting of multigraphene layers.[5] They can be produced economically by simple top-down approaches from abundantly existing and naturally available low-cost graphite. They are characterized by a 2D planar structure, an extremely high aspect ratio, and a remarkably large surface constant area.[6-8] Hence, GNPs are contemplated as ideal reinforcements for elastomers owing to their excellent balance of attributes and cost.[9] Normally the performance of elastomer-GNP composites largely depends on the degree of dispersion of the nanofillers and their interfacial compatibility with the elastomer matrix. However, the large surface area between GNPs leads to large Van der Waals forces and compelling interactions.[10-12] Consequently, the realization of graphene-based elastomer composites is limited by the aggregation and stacking of GNP sheets.

†To whom correspondence should be addressed.
prabu@ptuniv.edu.in, ORCID 0000-0003-2239-6635
©2026 The Polymer Society of Korea. All rights reserved.

Until the present time, numerous approaches have been employed to achieve better compatibility between the matrix and GNP, comprising the usage of polyelectrolytes and surfactants, which augment the dispersion of GNP in numerous matrices though electrostatic or physical interactions.[13] There are few research works reporting the enrichment of mechanical, electrical conductivity, thermal attributes and gas barrier in elastomers reinforced with GNPs, which are modified using several routes namely surfactants, ionic liquids, silane coupling agents like (3-aminopropyl)-tri-methoxysilane (APTMS) and grafting of functional groups, maleic anhydride, pyrene. Che *et al.*[14] have demonstrated momentous enhancement in modulus, thermal stability, swelling resistance and electrical conductivity in natural rubber (NR) composites filled with sodium sulphate dodecyl (surfactant) modified GNP. Gaca *et al*.[15] have divulged noteworthy enhancement in mechanical attributes, gas barrier characteristics and thermal stability of styrene butadiene rubber (SBR) composites incorporated with ionic liquid modified GNP through covalent grafting or non-covalent absorption. Scinski *et al*.[16] have reported noteworthy augmentation in SBR composites incorporated with low-temperature-plasma-modified GNP. Ren *et al*.[17] have explored the mechanical attributes and thermal conductivity of silicon rubber composites reinforced with (3-aminopropyl)-trimethoxysilane (APTMS)-modified GNP. Ganesh Kumar *et al*.[18] have reported enhanced mechanical attributes, swell characteristics, thermal resistance, dielectric characteristics and damping properties in EPDM composites with amine functionalized GNP(AGNP). Razzaq *et al*.[19] have presented a tremendous enhancement in solvent resistance and mechanical attributes of NR/EPDM composites incorporated with poly(ethyleneimine)-modified GNP. Yadav *et al*.[20] have demonstrated a noteworthy improvement of 600% in modulus and 30 °C in thermal stability in PU composites filled with hydroxyl functionalized GNP in comparison to pure PU. Cui *et al*.[21] adopted molecular dynamics (MD) simulations to compare the enhanced mechanical and tribological properties of nitrile rubber composites reinforced by different functionalized graphene sheets namely hydroxyl (OH), carboxyl (COOH), and ester ($COOCH_3$). Results revealed that Nitrile composites incorporated with COOH functionalized graphene demonstrated better mechanical and tribological attributes. Tao *et al*.[22] demonstrated better interface properties in COOH functionalized graphene filled vinyl silicone rubber (MVSR) composites in comparison to CH_3, OH and amine functionalized graphene filled MVSR composites for thermal interface applications. Hussain *et al*.[23] have demonstrated better young's modulus, shear modulus and bulk modulus in COOH functionalized graphene than ester functionalized graphene filled natural rubber composites using molecular dynamic simulations. A comparison of tensile strength, modulus and thermal conductivity of various rubber composites reinforced with different functionalised/Surface treated GNP summarised in Table 1.

It is highly evident from the literature that COOH-functionalized graphene provides a distinct advantage because the abundant carboxyl groups enhance compatibility with the rubber matrix, promote stronger interfacial interactions through hydrogen bonding and chemical coupling, improve filler dispersion, and suppress graphene restacking. These effects facilitate more efficient stress transfer from the rubber matrix to the graphene sheets, resulting in simultaneous improvements in tensile strength, modulus, thermal stability, and durability without requiring complex multi-step surface modification procedures. Consequently, COOH-functionalization represents a relatively simple and effective strategy for maximizing graphene reinforcement in rubber composites while maintaining good processability, making it an attractive alternative to other graphene functionalization approaches. However, there are very few studies that use specifically COOH-functionalized graphene (carboxylated graphene) as the reinforcing filler in rubber composites.

Bromobutyl rubbers (BIIR) are known for their superior thermo-oxidative stability, chemical and moisture resistance, low gas permeability, and vibration resistance.[24,25] These attributes qualify BIIR for making tire inner liners. Nonetheless, the absence of a covalent network structure in BIIR leads to inferior mechanical characteristics, especially low stiffness, poor stress at failure, and poor creep resistance. Hence, BIIR is often blended with NR to improve its mechanical attributes.[26-28] The development of lightweight fuel-eco-automobiles necessitates the development of rubber materials with improved isolation, high fatigue life, low elastic modulus, and good ride comfort. Blends of NR/BIIR are considered to be the fore runners to meet these requirements.[29] Le *et al*.[30] have developed self-healable materials based on butyl imidazole-modified BIIR-NR blends reinforced with CNTs. Chumnum *et al*.[31] have demonstrated self-healable composites with curing propagation, mechanical healing, morphologies, electrical conductivity, and recyclability together with suitable abrasion, rolling resistance, and wet traction based on butyl imidazole modified BIIR-NR blends reinforced with CNT and carbon black hybrid fillers. Nonetheless, studies describing the reinforcing effect of functionalized GNP on NR-BIIR blends are scarce.

Although graphene and functionalized graphene-based fillers have been extensively investigated in rubber composites,

Table 1. A Comparative Study for Tensile Strength, Elastic Modulus and Thermal Conductivity of Rubber Composites Reinforced with Different Functionalised/Surface Treated GNP from Literature

Methodology	Matrix	Reinforcement	Property studied	Value	% Improvement in property from matrix material
Experimental [13]	Natural rubber Latex	1phr of sodium sulfate dodecyl (SDS) treated GNP	Tensile strength	13MPa	1.5%
Experimental [14]	Styrene Butadiene rubber (SBR	5phr of 1-butyl-4-methylpyridinium tetrafluoroborate (BMPFB)	Tensile strength	4.7 MPa	117%
Experimental[15]	NR/EPDM	5% wt of poly(ethyleneimine)-modified GNP	Tensile strength		104%
Experimental [16]	Styrene Butadiene rubber (SBR)	Vinyltrimethoxy silane (VTMS) modified GNP	Tensile strength	6.5 MPa	26.7%
Experimental [16]	Styrene Butadiene rubber (SBR	Mercaptotrimethoxy silane (MTMS) modified GNP	Tensile strength	6.6 MPa	28.6%
Experimental [16]	Styrene Butadiene rubber (SBR)	low-temperature-plasma-modified GNP	Tensile strength	5.6 MPa	7.2%
Experimental [17]	Silicone rubber	2phr of (3-aminopropyl)-trimethoxysilane (APTMS)-modified GNP	Tensile strength	5.2 MPa	21%
Experimental [18]	EPDM	15phr of Amine functionalized graphene	Tensile strength	3.13 MPa	55%
Experimental [19]	NR/EPDM	1% wt of aminopropyltryetoxysilane (ATPS) modified GNP	Tensile strength	11.7 MPa	60.2%
Experimental [20]	Polyurethane	1.5%wt of hydroxyl functionalized GNP	Tensile strength	23.4 MPa	30.7%
Molecular dynamics [22]	Vinyl silicone rubber	Methyl functionalized GNP	Thermal conductivity	0.129 $Wm^{-1}K^{-1}$	135
Molecular dynamics [22]	Vinyl silicone rubber	Amine functionalized GNP	Thermal conductivity	0.122 $Wm^{-1}K^{-1}$	7%
Molecular dynamics [22]	Vinyl silicone rubber	hydroxyl functionalized GNP	Thermal conductivity	0.127 $Wm^{-1}K^{-1}$	12%
Molecular dynamics [22]	Vinyl silicone rubber	Carboxyl (COOH) functionalized GNP	Thermal conductivity	0.130 $Wm^{-1}K^{-1}$	14%
Molecular dynamics [23]	Natural rubber	Carboxyl (COOH) functionalized GNP	Elastic modulus	4.44 MPa	66.42%
Molecular dynamics [23]	Natural rubber	ester ($COOCH_3$) functionalized GNP	Elastic modulus	4.41 MPa	65.47%

most previous studies have focused on single-rubber matrices, graphene oxide, or alternative surface-functionalization strategies. In contrast, the present work investigates the reinforcement of an NR/BIIR blend using COOH-functionalized graphene nanoplatelets, where the carboxyl functional groups are expected to enhance interfacial compatibility with both rubber phases and improve filler dispersion. Unlike conventional graphene fillers, COOH-functionalized graphene provides enhanced interfacial interactions without the need for additional coupling agents or complex surface grafting. In this direction, an attempt is made to improve the performance of the composites using COOH-functionalized graphene nanoplatelets (FGNP) to improve the interactions such as enhanced filler-matrix adhesion, preventing phase separation and ensuring homo geneity with NR-BIIR matrices.

Hence in this research, an effort has been made to prepare NR-BIIR composites reinforced with COOH-functionalized GNP (FGNP). NR-BIIR composites containing 0, 1, 3, 5, 7, and 9 phr of FGNP were fabricated by melt-mixing on a twin-roll open mill. The morphology and the microstructure, were evaluated using field emission scanning electron microscopy (FESEM) and X-ray diffraction (XRD) studies. Furthermore, this study establishes a clear correlation between filler loading, morphology, and the resulting mechanical, thermal, and dynamic properties, thereby identifying an optimum loading that balances reinforcement and agglomeration. These findings provide practical

guidance for designing high-performance NR/BIIR composites for applications requiring enhanced mechanical durability, thermal stability, and barrier performance. Thus, beyond confirming established reinforcement trends, the present work demonstrates the effectiveness of COOH-functionalized graphene as a tailored interfacial modifier for NR/BIIR blends and offers application-relevant insights for the development of next-generation tire inner liner materials. The insights gained from these studies into filler–rubber interactions, chain mobility, and interfacial adhesion are expected to facilitate the design of inner liners with enhanced air retention, improved durability, and superior thermo-mechanical performance, thereby contributing to improved tire reliability and vehicle energy efficiency.

Experimental

Materials. COOH-functionalized graphene nanoplatelets (FGNP) were purchased from Adnano Technologies, Karnataka, India. Bromobutyl rubber (X2) was supplied by Lanxess Energising Chemistry (Germany). Natural rubber (RMA-1X) was procured from Manmeet Rubber Industries, Chennai. All the other compounding additives mentioned in Table 2 were provided by Ramcharan Company, Chennai.

Preparation of Composites. Table 2 shows the NR-BIIR composite formulas. A dual-roll mill with dimensions of 160 mm × 320 mm was used to compound the material. With the addition of NR-BIIR rubber to the mill, the blending process got underway. Following a few minutes of mastication, FG was added, and mixing was maintained for a further 10 minutes. The mixture was then supplemented with the antioxidant, activators (stearic acid), CB, and plasticiser and mixed for a further 20 minutes. Sodium stearate, potassium stearate, and sulphur were added last and combined for a further two to three minutes. It was possible to create a homogeneous compound. With 0, 1, 3, 5, 7, and 9% wt FGNP, six phr compounds were created. These compounds are first cured in an electric press at 160 °C. These vulcanisates were treated for various characterisations after being kept in an ambient environment for 24 hours.

Microstructure and Morphology. The morphology and microstructure of FGNPs and NR-BIIR composites were studied using a SUPRA 55 (CARL ZEISS, Germany) FESEM and a Rikagu Ultima IV X-ray diffractometer (Rikagu, Japan).

Raman Spectroscopy. FGNP was characterised using Raman spectroscopy (Renishaw Invia-Reflex, England, UK) utilising a 514 nm Ar laser.

FTIR Spectroscopy. FTIR was conducted using a Cary 630 FTIR analyser (Agilent Technologies, USA) in the range of 400 to 4000 cm^{-1}.

Tensile and Tear Tests. Compression-molded sheets with a thickness of approximately 2 mm are used for determining tensile and tear attributes. According to ASTM D412, standard dumbbell-shaped specimens are utilized to calculate tensile strength. According to ASTM D624, the tear strength of composites is measured using un-nicked test specimens. Both these tests are conducted using an Instron Universal Tester (Model 4301); the test is performed with an initial clamp spacing of 65 mm and a crosshead speed of 500 mm/min.

Hardness and Abrasion Tests. In line with ASTM D2240, the hardness of the composites is assessed using a Shore A durometer. Abrasion loss was determined using an abrasion tester

Table 2. Formulation of NR-BIIR Composites (Phr)

Ingredients (Phr[a])	Gum	FGNP1	FGNP3	FGNP5	FGNP7	FGNP9
NR	50	50	50	50	50	50
BIIR	50	50	50	50	50	50
Zinc oxide	5	5	5	5	5	5
Stearic acid	1	1	1	1	1	1
TDQ[b]	2	2	2	2	2	2
FGNP	0	1	3	5	7	9
Napthenic oil[c]	2	2	2	2	2	2
Sulphur MC	1.5	1.5	1.5	1.5	1.5	1.5
MC Wax[d]	2	2	2	2	2	2
MBTS[e]	1.5	1.5	1.5	1.5	1.5	1.5
TMTD[f]	0.2	0.2	0.2	0.2	0.2	0.2

[a]Parts by weight per hundreds of rubbers; [b]2,2,4-trimethyl-1,2-dihydroquinoline (Antioxidant); [c]Processing oil; [d]Antiozonant; [e]Mono benzothiazole disulfide (Primary Accelerator); [f]Tetramethyl Thiuram Disulfide (Secondary Accelerator)

(Make: Prolific Engineers) in accordance with ASTM D5963.

Thermo-Oxidative Resistance. As per ASTM D573-99, the hot-air ageing resistance is evaluated for 72 hours in a hot air oven set to 100 °C. Servo enterprises (SERVO-15) are shown in Figure 2. For each of the NR composites examined, five sets of specimens were evaluated under various ageing circumstances. Stress at rupture and elongation at failure have been determined post-ageing to evaluate ageing resistance. The percentage of retention in properties of the specimens is evaluated as follows:

$$\% \text{ property retention} = \frac{\text{Property post aging}}{\text{Property prior ageing}} \quad (1)$$

Interfacial Interactions and Thermal Stability. Interfacial interactions between FGNP and NR-BIIR are evaluated using a DMA analyser (6100, SIINANO technology, Japan). Storage modulus and tan delta were determined in the range from -100 °C to 100 °C at a heating rate of 5 °C/min, a frequency of 1 Hz and a strain of 0.2%. Thermogravimetric studies were conducted using a TGA analyser (6100, SIINANO technology, Japan) from ambient temperature to 600 °C.

Results and Discussions

Chemical Structure and Morphology of FGNP. The FTIR spectra of FGNP are presented in Figure 1(a). The peaks observed at 1050, 1275, 1698, and 3445 cm^{-1} confirm the presence of various functional groups on the surface of FGNP, including C-O-C (epoxy group), C-O (alkoxy), C=O (carbonyl), C=O-OH

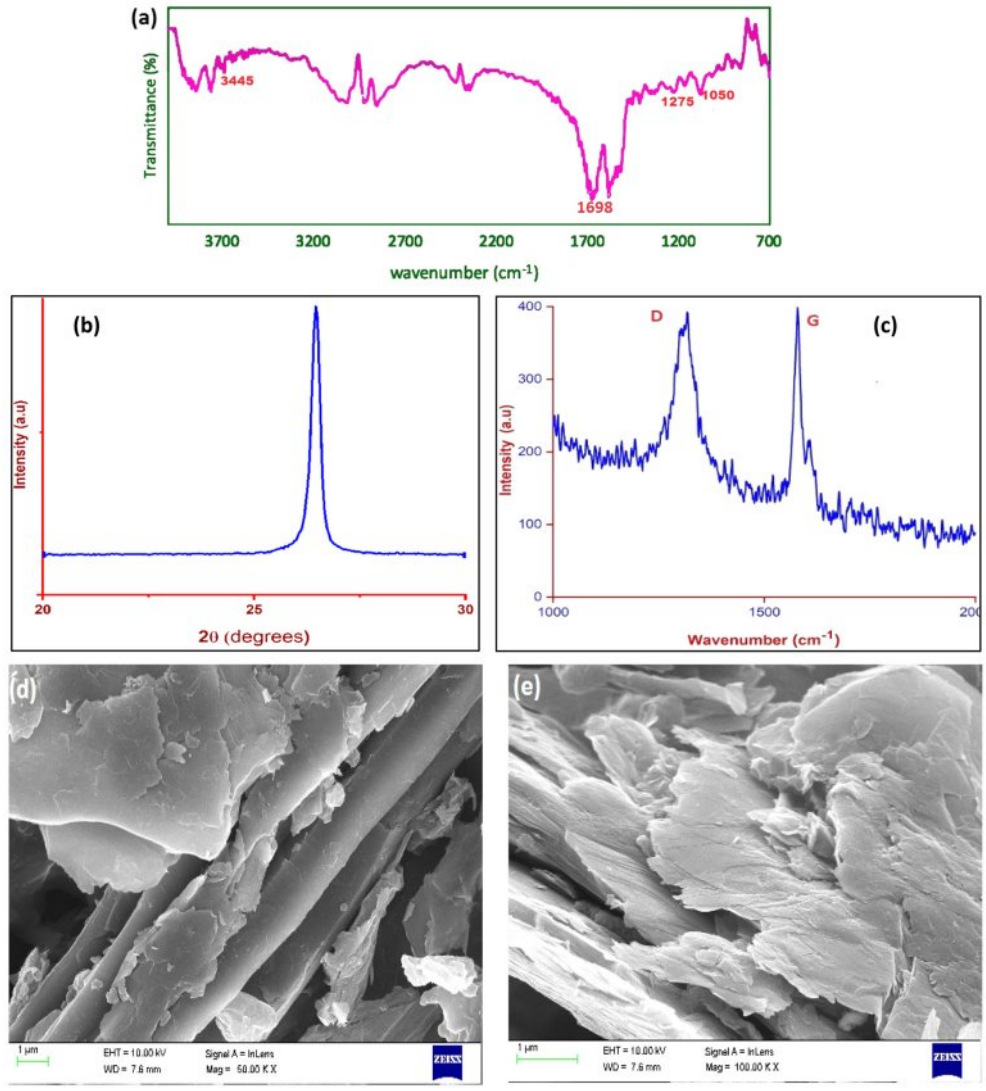

Figure 1. (a) FTIR spectra; (b) XRD spectra; (c) Raman spectra; (d),(e) FESEM at different magnification of COOH-functionalized Graphene nanoplatelets (FGNP).

(carboxyl), and –OH (hydroxyl group).[32] The presence of these specific functional groups alters the surface charges. The XRD spectra of FGNP are shown in Figure 1(b). It is evident that FGNP exhibits a diffraction peak at 2θ=26.4691°, which corresponds to the 0 0 2 basal plane, indicating the stacking of a single graphene layer with a spacing of 0.336 nm.[33] Figure 1(c) displays the Raman spectra of FGNP. As is typical for graphitic-based materials, it shows a D band at 1319 cm^{-1} and a G band at 1579 cm^{-1}. Additionally, the G band features a shoulder at 1620 cm^{-1}, suggesting the formation of sp^3 bonds due to the functional groups attached to the FGNP surface.[34,35] Figures 1(d) and 1(e) present FESEM images of the COOH functionalized graphene (FGNP) prior to its incorporation into the rubber matrix. These FESEM images reveal numerous flakes of varying shapes and sizes. At higher magnification (Figure 1(d)), the stacks of particles appear thinner and seem to be interconnected at the edges of the platelets. Furthermore, as illustrated in Figure 1(e), the specific graphite nanosheet comprises several layers of graphene sheets rather than being a single graphite nanosheet or simply "graphene."

Structural Characterization. Figure 2 displays the XRD patterns of NR-BIIR composites. Furthermore, the 002 peak of FGN is slightly shifted, and its intensity is reduced in the XRD spectra of NR-BIIR composites with 1-5 phr FGNP, as can be observed in Figures 2(b-d). This reduction in intensity may be attributed to the tendency of graphene sheets to become more randomly oriented and aligned, resulting in a higher likelihood of uniform scattering.[36] Conversely, the peak intensity increases in NR-BIIR composites with 7 phr FGNP, as presented in Figure 2(e). This phenomenon demonstrates the inability of FGNP to disperse completely or separate, indicating the presence of a few layers in stacked form. Additionally, the intensity of the peak further increases in NR-BIIR composites with 9 phr FGNP (Figure 2(f)), suggesting the presence of more layers in stacks.[37]

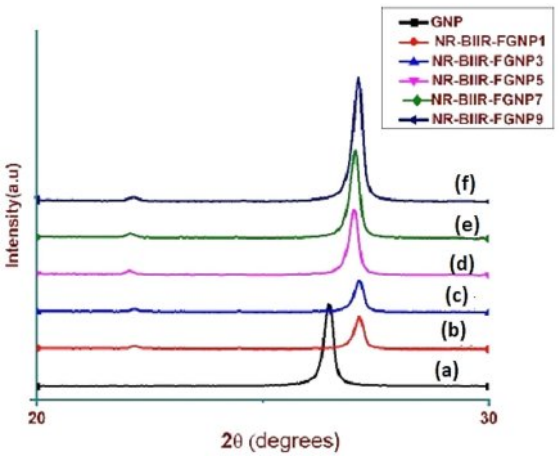

Figure 2. XRD spectra of (a) FGNP; (b) BIIR-FGNP1; (c) NR-BIIR-FGNP3; (d) NR-BIIR-FGNP5; (e) NR-BIIR-FGNP7; (f) NR-BIIR-FGNP9 composites.

Table 3. Characteristic Bands of Natural Rubber (NR), Bromobutyl Rubber (BIIR) and Functionalized Graphene Nanoplatelets in NR-BIIR-FGNP Composites

Wavenumber (cm^{-1})	Functional group mode
3445	OH (hydroxyl group) in FGNP
2963	CH_3 asymmetric stretching in NR
2917	CH_2 asymmetric stretching in NR
2849	CH_2 symmetric stretching in NR
1665	C=O-OH (carboxyl)in FGNP
1654	C=C stretching in NR
1437	CH_2 deformation in NR
1371	CH_3 deformation in NR
1275	C-O (alkoxy) in FGNP
1144	C-C stretching in BIIR
1458	C-H in plane bending in BIIR
1050	C-O-C (epoxy group) in FGNP
1024	C-H out of plane bending in BIIR
832	=C-H out of plane bending in NR
566	NR main chain deformation

Figure 3 and Table 3 present the FTIR spectra for NR, BIIR, and NR-BIIR-FGNP composites. In Figure 3(a), the distinctive peaks of NR are observed at 2963, 2917, 2849, and 1594 cm^{-1}, which correspond to the stretching vibrations of CH_3, asymmetric CH_2, symmetric CH_2, and C=C, respectively.[38] Furthermore, specific peaks of NR at 1449, 1375, and 832 cm^{-1} are attributed to the asymmetric and symmetric C-H stretching vibrations and C=H out-of-plane bending.[38] The peaks at 1458, 1024, and 1144 cm^{-1} in BIIR are associated with the in-plane bending and out-of-plane bending vibrations of C-H and C=C stretching, as shown in Figure 3(b).[39] The intensity of the C=C peak at 1594 cm^{-1}, originating from the polyisoprene unit in NR-BIIR composites, is noted to decrease as the FGNP concentration increases from 1 to 5 phr, as depicted in Figures 3(c-h). The FTIR measurements indicate clearly that there is no chemical interaction between FGNP and NR-BIIR; only physical interactions are present.[40]

Dispersion State of FGNP in NR-BIIR Composites. Figure 4 shows the cross-sectional morphology of the FG-NR-BIIR nanocomposite at varying FG loading levels of 3, 5, 7, and 9 phr, captured at low (500×), high (3500×), and very high (20000×) magnifications. As illustrated in Figures 4(a-d),

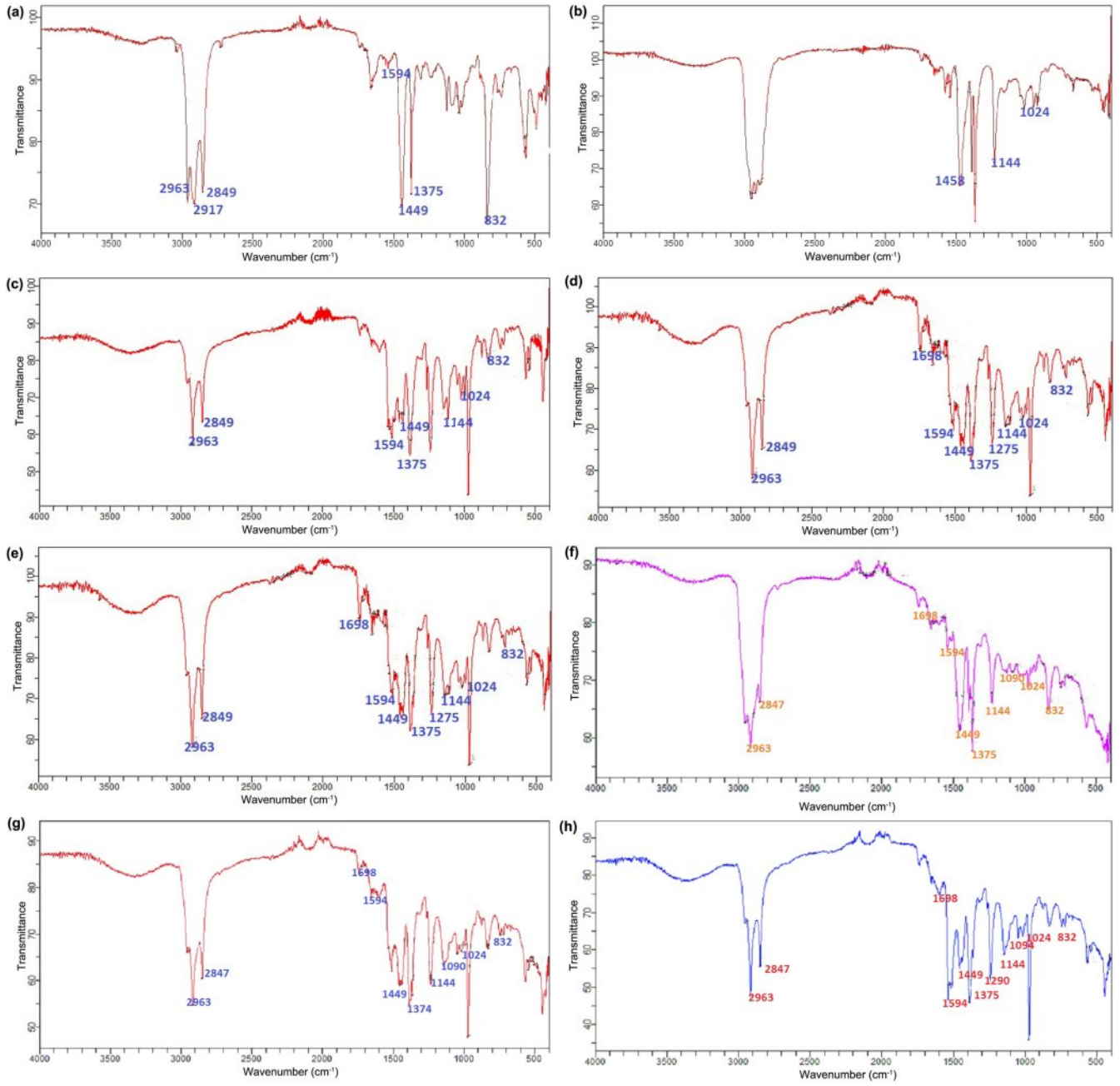

Figure 3. FTIR spectra of (a) natural rubber; (b) bromobutyl rubber, (c) NR-BIIR-gum; (d) NR-BIIR-FGNP1; (e) NR-BIIR-FGNP3; (f) NR-BIIR-FGNP5; (g) NR-BIIR-FGNP7; (h) NR-BIIR-FGNP9 composites.

increasing the FGNP loading from 0 to 5 phr results in a more random orientation and more uniform dispersion of FGNP within the NR-BIIR matrices.[41,42] This enhancement is attributed to the favorable contact and interfacial adhesion between the NR-BIIR rubber matrices and FGNP, which leads to improved mechanical and thermal stability of the nanocomposite. However, for FGNP loading levels exceeding 5 phr, the FGNP become more ordered and stacked, leading to a more heterogeneous and agglomerated structure of the nanocomposite, as depicted in Figures 4(e-h).[43] As a result, there is a decline in both mechanical and thermal properties.

Interfacial Interactions Between FGNP and NR-BIIR Blends. DMA study of the NR-BIIR composites was done to look at the interfacial interactions between the FGNP and the NR-BIIR matrix. Figure 5(a) and Table 4 display the curves of storage modulus (E') and loss tangent (tan) with temperature.

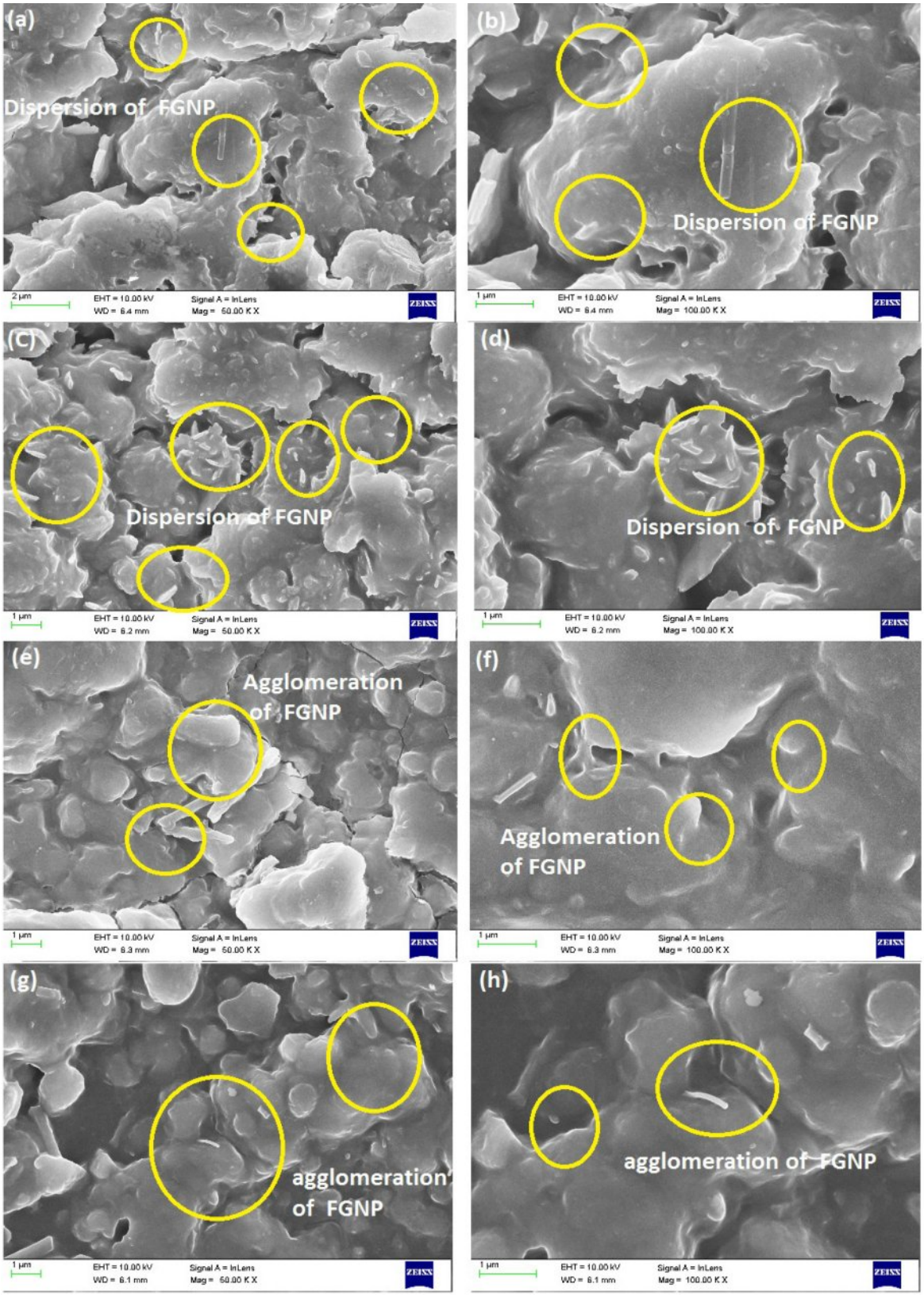

Figure 4. FESEM images of (a),(b) NR-BIIR-FGNP3; (c),(d) NR-BIIR-FGNP5; (e),(f) NR-BIIR-FGNP7; (g),(h) NR-BIIR-FGNP9 composites at different magnifications.

It's worth noting that the incorporation of FGNP filler to the NR-BIIR matrix results in a remarkable enhancement in E'.

When compared to a NR-BIIR gum, all NR-BIIR-FGNP nanocomposites are always shown to have E' values that are higher at all temperatures. In comparison to gum, at the same temperature, the storage modulus of NR-BIIR composites containing 1, 3, 5, 7, and 9 phr of FGNP increased by 36, 411, 401, 111, and 11% at 30 °C. For a given filler quantity, the E' value is mostly controlled by the interfacial contact between the filler and rubber. The increased value of E' indicates the establishment of a strong interfacial contact between the FGNP and the NR-BIIR matrix, which allows stress to be transferred from the NR-BIIR matrix to the FGNP sheets.[31,43]

Effect of FGNP fillers on the mobility of the elastomeric chains was studied by dynamic mechanical analysis (DMA). The energy dissipation in the glass transition is governed by the viscous motion of the long-range polymer chains, which is shown by the loss factor (tan δ). As demonstrated in Figure 5(b), the height of tan δ peak shows the damping ability and mobility of the polymer segments. The decrease in the peak height of tan δ suggests limited polymer chain mobility due to enhanced filler–matrix interactions. This constraint is often connected with enhanced interfacial adhesion in elastomeric composites. The tan δ peak heights of all the NR-BIIR-FGNP composites were lower than those of the NR-BIIR gum, which confirms the improved interfacial adhesion between the FGNP filler and the NR-BIIR matrix.[44] Among the composites, the lowest tan δ peak was seen for the specimen with 5 phr FGNP, indicating the highest restriction of polymer chain mobility and the strongest contact between filler and matrix.

The glass transition temperature (T_g) was obtained from the temperature corresponding to the maximum tan δ peak in Figure 5(b). The NR-BIIR gum had T_g value of -33.1 °C and all NR-BIIR-FGNP composites showed a change in T_g to higher temperatures. The composite with 5 phr FGNP showed the highest T_g (-29.5 °C), which suggested that the homogenous dispersion of FGNP and increased interfacial bonding could effectively constrain the mobility of the molecular chains of the NR-BIIR.[43,45] However, the 7 and 9 phr FGNP composites displayed slightly lower T_g values than the 5 phr composite. This

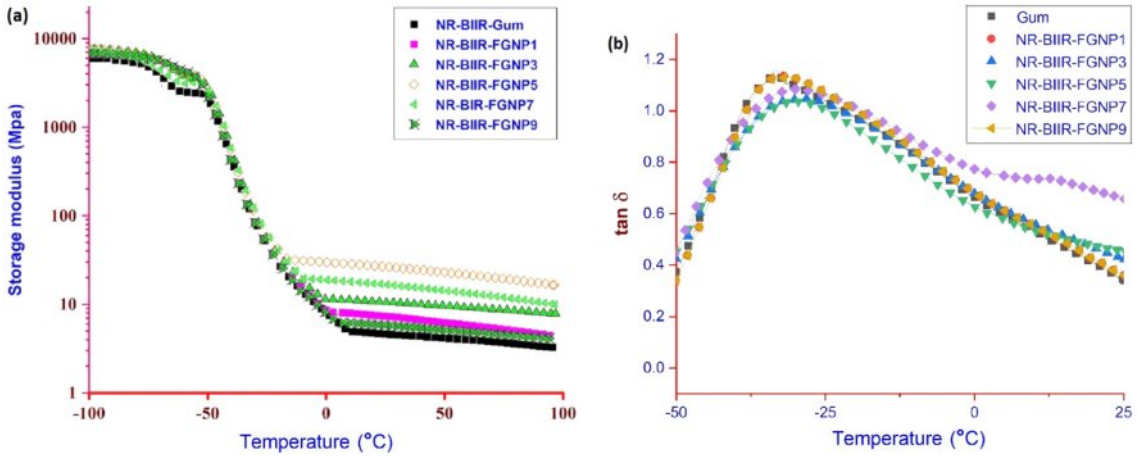

Figure 5. Variation of (a) Storage modulus (E') with temperature; (b) variation of loss factor (tan δ) with temperature for NR-BIIR-FGNP composites.

Table 4. DMA Characteristics of NR-BIIR Composites

Samples	Storage modulus (MPa) at different temperatures (°C)						T_g (°C)
	-70	-50	-30	30	50	70	
NR-BIIR-Gum	3905.63	2130.36	85.81	1.81	0.83	0.47	-33.1
NR-BIIR-FGNP1	5530.21	2527.91	95.07	2.47	1.50	1.48	-32.4
NR-BIIR-FGNP3	5687.34	2838.41	105.72	9.07	8.12	7.34	-31.9
NR-BIIR-FGNP5	5705.26	2741.95	119.14	9.37	10.4	5.28	-29.5
NR-BIIR-FGNP7	5654.605	2701.02	115.50	3.83	2.30	1.36	-30.4
NR-BIIR-FGNP9	5626.504	2421.02	83.53	2.01	1.04	0.26	-32.6

phenomenon can be explained by the production of FGNP agglomerates at filler loadings over 5 phr resulting in increased free volume in the matrix and polymer chain motion leading to a reduction in T_g of the NR-BIIR composites.[46]

Crosslinking Characteristics. The rate at which the FGNP particles crosslink in the NR-BIIR matrix is directly impacted by their dispersion. Figure 6 presents the crosslinking characteristics of several composites are displayed. There are studies in the literature which state that functional groups present on the surface of the carbon nanofillers can absorb the basic accelerator and delay the onset of vulcanization. In our study, the ideal cure time (t_{90}) was shown to decrease as FGNP concentration increased, supporting greater FGNP dispersion inside the NR-BIIR matrix (Figure 6(a)). The higher thermal conductivity and the larger surface area of FGNP facilitates easy flow of heat and result in sooner completion of the cure process.[46,47] It is also stated that FGNP adsorbs accelerators on its surface and acts as physical barriers to the sulphur accelerator reaction and the formation of zinc-accelerator complex, resulting in reduction of overall cure time.[48] Similar trend is also observed with scorch time (t_{s2}.) upon FGNP addition in the NR-BIIR matrix (Figure 6(a)).

Figure 6(b) demonstrate the maximum and minimum torques of NR-BIIR-FGNP nanocomposites. The viscosity arising from the tensions between the raw rubber molecular chains before curing is implied by the minimum torque value (ML), or ML. A measurement of the cross-link density of cured rubber is the maximum torque value (MH). The rheometer was used to measure the MH and ML. It is clear that the ML and MH values of the NR-BIIR-FGNP composites increased up to 5 phr, peaking at 5 phr FGNP, and subsequently decreased when the FGNP concentration was raised further. This revealed that the strongest rubber molecular chain and FGNP contacts occurred at 5 phr of FGNP nanofillers, which may be ascribed to the highest filler matrix adherence.[43] The agglomeration of the FGNP, which results in poor interaction between the NR-BIIR and FGNP, contributes to the drop in ML and MH values after 5 phr FGNP concentration.[43]

Cure rate index (CRI) is an indicator of the rate of vulcanisation and is calculated based on the differences between. t_{90} and t_{s2}. It can be noted that CRI is increased for NR-BIIR composites loaded with FGNP, as presented in Figure 6(c). This can be attributed to the filler's capacity to quicken the vulcanization process. Additionally, as the cure progresses, FGNP and NR-BIIR may have reacted, producing new cross-links or network structures inside the composite material. By preventing

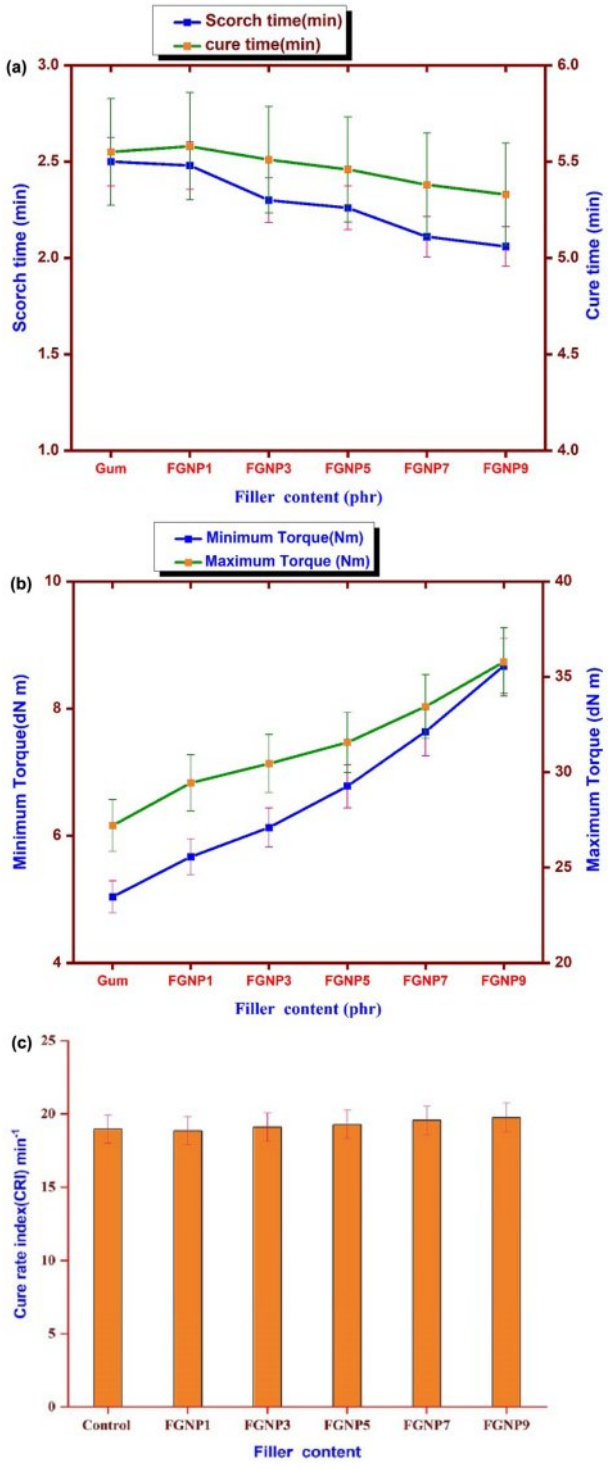

Figure 6. (a) Scorch time and cure time; (b) minimum and maximum torque; (c) cure rate index of NR-BIIR-FGNP composites.

extended relative movement of the chains, these networks in turn increased the stiffness of the nanocomposites. The torque differential values may have increased as the content of the FGNP increased due to this event. The vulcanization rate of the

NR-BIIR-FGNP composites improves noticeably, and the cure rate index (CRI) is improved by a factor of 2.6. Such an improvement is credited to the FGNP's improved dispersion in BR composites. Similar results for CRI are observed in graphene reinforced natural rubber composites.[49] The enhanced values of CRI also indicate the decreased energy of activation for crosslink formation and augmented interaction for curing.[18,50]

Mechanical Characteristics. By examining the data presented, it can be noted that the tensile strength of BIIR/NR nanocomposites is more than that of conventional composites by 6.9, 12.9, 22.9, 14.8, and 5.1% respectively, for 1, 3, 5, 7, and 9 phr of GNP content in the NR/BIIR hybrid nanocomposites. Further from Figure 7(a), it can be noted that in NR/BIIR hybrid nanocomposites, the tensile strength increases upto 5 phr FGNP content and thereafter decreases with further increase in GNP content. Such an improvement in tensile strength may be accredited to (i) the greater surface area of FGNP and its improved interaction with the BIIR-NR matrix,[52] (ii) Presence of COOH group's presence on the graphene layers' surface obstructed their stacking and enhanced the dispersion of FGNP in the rubber blend.[53] Enhanced dispersion of FGNP and augmented BIIR-NR-FGNP interactions enabled more efficient transfer of stress at the interface and hence improved tensile performance.[14] Tensile strength decreases at 5 phr of nanofiller content because of poor rubber-filler interaction and restacking of graphene layers.[54–55]

It is also evident from Figure 7(b) that NR/BIIR nanocomposites incorporated with 1, 3, 5, 7, and 9 phr of FGNP content, respectively, exhibited 6.3, 8.6, 19, 5.1, and 2.5% increase in % ER in comparison to NR-BIIR gum. It has been normally observed that loading of composites with fillers leads to a reduction in ER.[56] Nonetheless, a reversed trend was noticed in the studied composites. Further from Figure 7(b), it can be noted that in NR/BIIR composites, the ER increases up to 5 phr FGNP content and thereafter decreases with further increase in FGNP content. The significant augmentation in ER can be attributed to

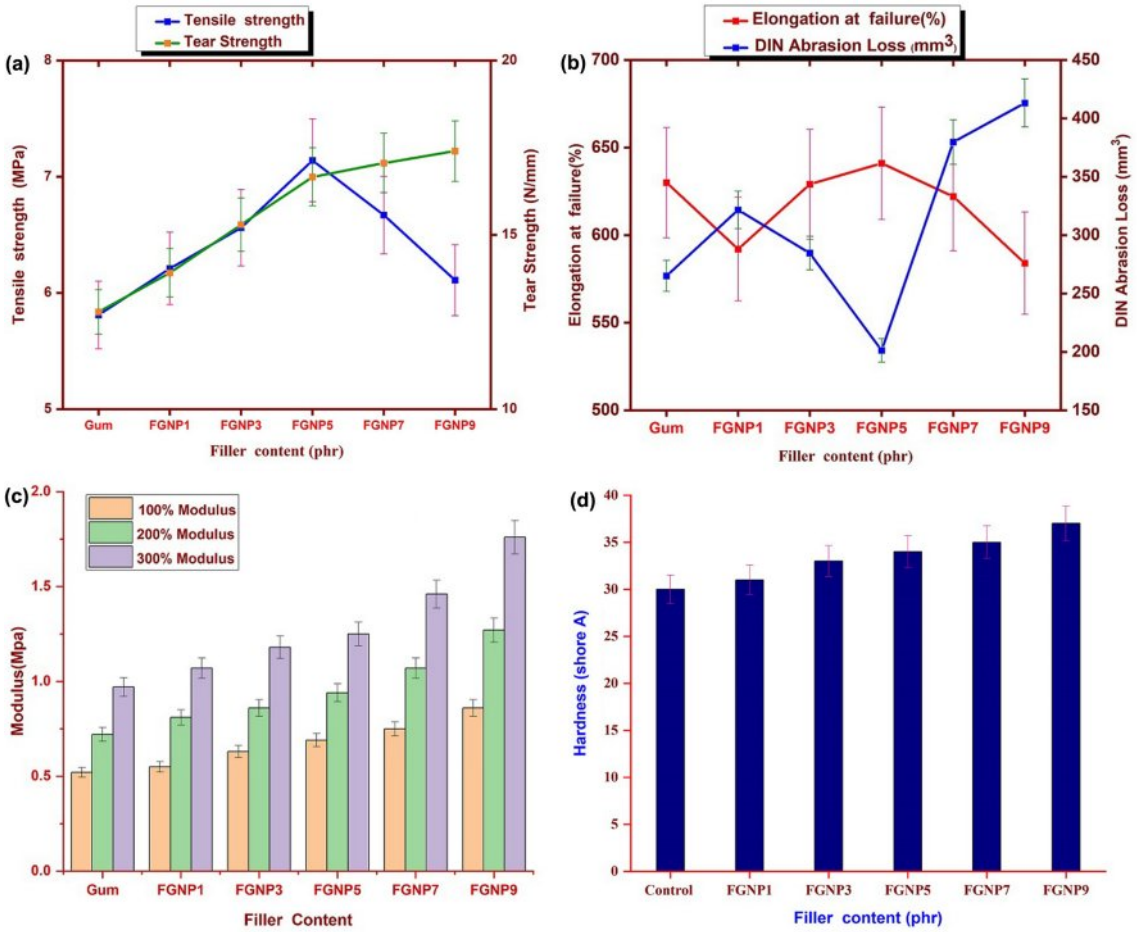

Figure 7. (a) stress at rupture and tear strength; (b) elongation at failure and abrasion loss; (c) tensile modulus at 100%, 200% and 300% strain of NR-BIIR-FGNP; (d) hardness of NR-BIIR-FGNP composites.

the susceptibility of FGNP to disturb the physical crosslinking sites of the NR-BIIR blends and promoting elastomer chain movement.[14] Hence, the developed NR-BIIR composites exhibited greater strength and superior extensibility.

It can be noted from Figure 7(c) that NR-BIIR composites demonstrate a remarkable increase in modulus with an increase in FGNP loading from 1-9 phr. The modulus of NR-BIIR composites with 9 phr FGNP presented an improvement of 65.3, 76.3, and 81.4% respectively at strain levels of 100, 200, and 300%, in comparison to gum. Such a significant improvement in modulus can be attributed to the proficient transfer of load between FGNP and NR-BIIR blends.[57]

The simultaneous increase in modulus and elongation at break with increasing loading of COOH-functionalized graphene in the NR/BIIR blend can be attributed to the homogeneous dispersion of the functionalized graphene and its strong interfacial interaction with the rubber matrix. The carboxyl-functionalized graphene enhances stress transfer and forms an effective reinforcing network, thereby increasing the stiffness of the composite. In addition, the functionalized graphene improves the compatibility between the NR and BIIR phases by preferentially localizing at the blend interface, leading to a finer and more uniform morphology. The uniformly dispersed graphene also delays crack initiation and propagation through crack-bridging and crack-deflection mechanisms, while the NR phase undergoes efficient strain-induced crystallization during stretching. These synergistic effects enhance both the modulus and elongation at break up to an optimum graphene loading. Results similar to our work with simultaneous increase in elongation at break and modulus have been reported by Mondal *et al.*[58] in acrylonitrile butadiene composites. Elongation at break and modulus at 300% were reported to increase by with increase in graphene nanoplatelets loading from 0 to 20 Phr.

NR-BIIR composites demonstrate augmentation in hardness values with enhancement in FGNP loading from 1-9 phr (Figure 7(d)). The better results can be ascribed to more uniform dispersion of FGNP, stronger NR-BIIR-FGNP interactions, a higher modulus of FGNP, and the formation of additional crosslinks between rubber and filler.[43,59] A considerable reduction in abrasion loss values of NR-BIIR composites can be noticed in Figure 7(b) till the incorporation of 5 phr FGNP content. The NR-BIIR-FGNP5 composite recorded the highest decline of 24% among the various composites studied. The results can be accredited to enhanced dispersion of FGNP and augmented BIIR-NR-FGNP interactions.[31] Furthermore, the tear resistance of NR-BIIR nanocomposites is improved by 8.7, 19.5, 30.2, 33.3, and 36.1%, respectively, for 1, 3, 5, 7, and 9 phr FGNP concentration (Figure 7(a)). It is obvious that the tear resistance of NR-BIIR nanocomposites increases up to 5 phr FGNP and then decreases with further enhancement in FGNP content. The exceptional performance of NR-BIIR nanocomposites is due to (i) the large size of platelets and their intrinsic geometrical attributes and (ii) improved adhesion between FGNP and NR-BIIR. These factors offer strong resistance to crack initiation and propagation, endorse efficient transfer of load from NR-BIIR blends, and prevent failure at low stress levels.[60,61]

Hot Air Ageing. Figure 8(a) shows the tensile strength of conventional and hybrid NR/BIIR nanocomposites before and after hot air ageing for 70 hours at 100 °C. These findings show that hot air ageing reduces the tensile strength of both conventional

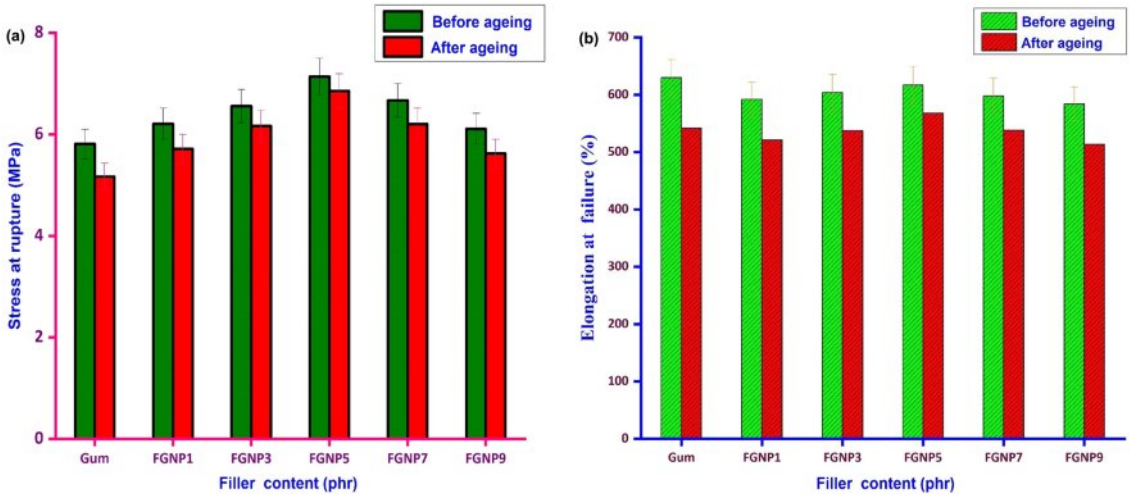

Figure 8. (a) stress at rupture; (b) elongation at failure of NR-BIIR gum and NR-BIIR-FGNP Composites after hot air ageing at 100 °C for 70 h.

and hybrid NR/BIIR nanocomposites. This is caused by the primary NR/BIIR chains degrading as a result of ageing.[62] After being aged in hot air, 89% of the tensile strength was retained in the NR/BIIR conventional composite. After hot air ageing, the percentages of tensile strength retained for 1, 3, 5, 7, and 9 phr GNP content in NR/BIIR hybrid nanocomposites are 92, 94, 96, 93, and 92%, respectively. This leads to the conclusion that, after being aged in hot air, NR-BIIR nanocomposites had greater tensile strength than gum

Figure 8(b) shows the per cent elongation at failure of NR-BIIR composites before and after 70 hours of hot air ageing at 100 °C. The results illustrate that NR-BIIR composites experience a decrease in elongation at failure during hot air ageing. This decrease in % elongation at failure is caused by chain scission, which weakens the primary NR/BIIR chains.[63] After hot air ageing, the NR/BIIR gum shows an 86% preservation of elongation at rupture. After being aged in hot air, NR/BIIR hybrid nanocomposites containing 1, 3, 5, 7, and 9 phr of GNP showed enhanced retention of % elongation at break of 88, 89, 92, 90, and 88%, respectively. Increased NR-BIIR-CB-GNP interactions and intercalated structure creation promote a convoluted route that reduces oxygen absorption and increases hot air ageing resistance. For natural rubber-carbon black organoclay hybrid nanocomposites, similar outcomes are reported.[64]

Thermal Stability. Figure 9 and Table 5 present the thermogravimetric (TGA) attributes of BIIR-NR-FGNP composites. The TGA parameters, namely temperatures at 10% weight loss, 50% weight loss, maximal degradation temperature, and char residue weight at 600 °C of the prepared composites, are explored, and the data are presented in Table 5. It is highly evident that in all the TGA parameters of NR-BIIR-FGNP composites were greater than those of the gum. NR-BIIR composite with 9 phr FGNP demonstrated superior TGA parameters (T_{10} at 328.5 °C, T_{50} at 393.6 °C, and char residue percentage of 13.6%) among the various composites investigated. Inherent capability of FGNP to prevent heat propagation, better FGNP dispersion across the NR-BIIR matrix and improved NR-BIIR-FGNP interactions served to reduce the diffusion of generated degradation gases, which in turn serve to prevent additional NR and BIIR degradation.[64-67]

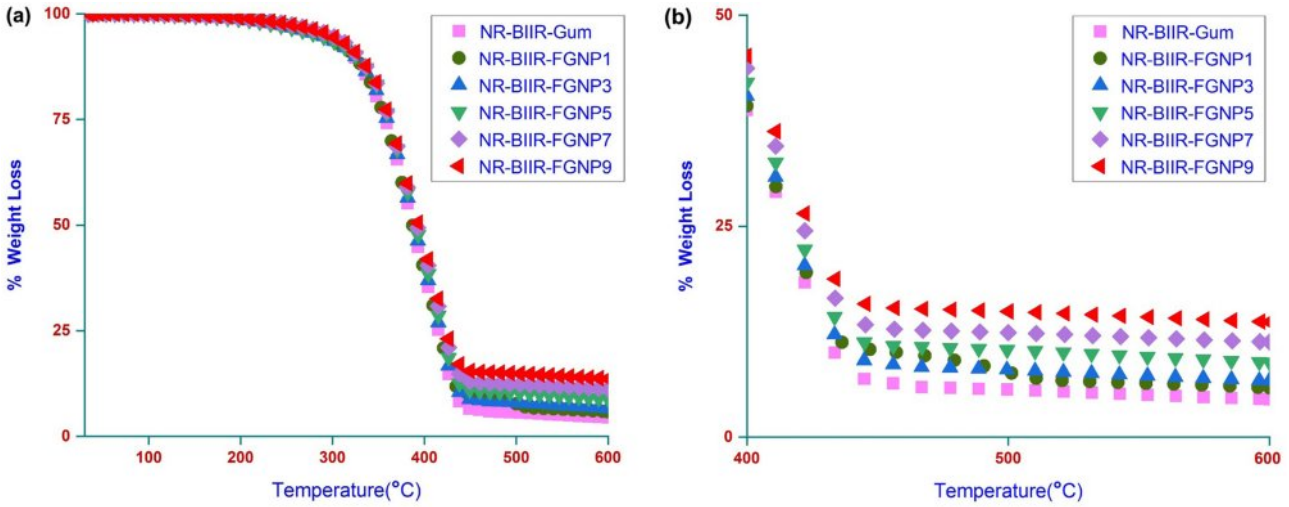

Figure 9. (a), (b) Thermogravimetric curves of NR-BIIR-FGNP composites at the heating rate of 10 °C/min under nitrogen atmosphere.

Table 5. Thermogravimetric Analysis (TGA) Data of NR–BIIR Nanocomposites, Showing the Onset Decomposition Temperature (T_{10}%), Temperature at 50% Degradation Rate (T_{50}%), Residual Char Content at 600 °C

Composites	T_{10}% (°C)	T_{50}% (°C)	Char residue weight (%) at 600 °C
NR-BIIR-Gum	323.2	387.1	4.4
NR-BIIR-FGNP1	323.6	387.5	5.8
NR-BIIR-FGNP3	324.4	388.7	6.7
NR-BIIR-FGNP5	325.7	390.3	8.9
NR-BIIR-FGNP7	327.7	392.1	11.3
NR-BIIR-FGNP9	328.5	393.6	13.6

Conclusion

In this research work, an effort has been made to prepare and characterize NR-BIIR composites containing 0-9 phr FGNP. These composites were prepared by melt blending on a two-roll open mill. The prepared composites demonstrated remarkable improvement in mechanical attributes, thermal stability and dynamical mechanical characteristics in comparison to their gum. Further NR-BIIR composites incorporated with 5 phr FGNP presented an improvement of 22.9, 19, 32.6, 30.2, and 24% respectively in stress at rupture, elongation at failure, 100% modulus, tear strength and abrasion loss respectively. The thermogravimetric characteristics namely (temperatures at 10% weight loss (T_{10}) and 50% weight loss (T_{50}) and char residue concentration at 600 °C of 5 phr FGNP reinforced NR-BIIR composites are 2.5, 3.2 °C and 102% higher than that of NR-BIIR gum. The interfacial adhesion between FGNP and NR-BIIR was confirmed by the remarkable enhancement in storage modulus (E') and the glass transition temperature (T_g) of NR-BIIR-FGNP composites. Uniform dispersion of FGNP in NR-BIIR matrix as evinced by FESEM and XRD studies and improved compatibility between FGNP and NR-BIIR resulted in augmented mechanical characteristics and thermal stability of NR-BIIR-FGNP composites.

Acknowledgments. The authors would like to express their gratitude to Tech Centre, Ramcharan Chemicals, Chennai, and KELVN Labs, Hyderabad, for assisting them with sample preparation and testing.

Conflict of Interest: The authors declare that they have no conflict of interest.

References

1. Geim, A. K.; Novoselov, K. S. The Rise of Graphene. *Nat. Mater.* **2007**, 6, 183-191.
2. Stankovich, S.; Dikin, D. A.; Dommett, G. H. B.; et al. Graphene-Based Composite Materials. *Nature* **2006**, 442, 282-286.
3. Ponnamma, D.; Sadasivuni, K. K.; Strankowski, M.; Guo, Q.; Thomas, S. Synergistic Effect of Multiwalled Carbon Nanotubes and Reduced Graphene Oxides in Natural Rubber for Sensing Application. *Soft Matter* **2013**, 9, 10343-10353.
4. Bhattacharya, M.; Biswas, S.; Bhowmick, A. K. Permeation Characteristics and Modeling of Barrier Properties of Multifunctional Rubber Nanocomposites. *Polymer* **2011**, 52, 1562-1576.
5. Li, B.; Zhong, W. H. Review on Polymer/Graphite Nanoplatelet Nanocomposites. *J. Mater. Sci.* **2011**, 46, 5595-5614.
6. Chen, G. H.; Wu, D. J.; Weng, W. G; Yan, W. L. Preparation of Polymer/Graphite Conducting Nanocomposite by Intercalation Polymerization. *J. Appl. Polym. Sci*. **2001**, 82, 2506-2513.
7. Weng, W. G.; Chen, G. H.; Wu, D. J.; Yan, W. L. HDPE/Expanded Graphite Electrically Conducting Composite. *Compos. Interfaces* **2004**, 11, 131-143.
8. Li, J.; Kim, J. K. Percolation Threshold of Conducting Polymer Composites Containing 3D Randomly Distributed Graphite Nanoplatelets. *Compos. Sci. Technol*. **2007**, 67, 2114-2120.
9. XG Sciences, Inc. XG Sciences. Available at: http://www.xgsciences.com (accessed November 15, 2025).
10. Si, Y.; Samulski, E. T. Exfoliated Graphene Separated by Platinum Nanoparticles. *Chem. Mater*. **2008**, 20, 6792-6797.
11. Si, Y.; Samulski, E. T. Synthesis of Water-Soluble Graphene. *Nano Lett*. **2008**, 8, 1679-1682.
12. Li, D.; Müller, M. B.; Gilje, S.; Kaner, R. B.; Wallace, G. G. Processable Aqueous Dispersions of Graphene Nanosheets. *Nat. Nanotechnol*. **2008**, 3, 101-105.
13. Che, W. M.; Teh, P. L.; Yeoh, C. K.; Abd Jalil, J. B.; Lim, B. Y.; Rasidi, M. S. M. Effect of Dispersibility of Graphene Nanoplatelets on the Properties of Natural Rubber Latex Composites Using Sodium Dodecyl Sulfate. *e-Polymers* **2022**, 22, 752-762.
14. Gaca, M.; Vaulot, C.; Maciejewska, M.; Lipińska, M. Preparation and Properties of SBR Composites Containing Graphene Nanoplatelets Modified with Pyridinium Derivative. *Materials* **2020**, 13, 5407.
15. Abd Razak, J.; Haji Ahmad, S.; Ratnam, C. T.; Mahmood, M. A.; Mohamad, N. Effects of Poly(ethyleneimine) Adsorption on Graphene Nanoplatelets to the Properties of NR/EPDM Rubber Blend Nanocomposites. *J. Mater. Sci*. **2015**, 50, 6365-6381.
16. Siciński, M.; Bieliński, D. M.; Szymanowski, H.; Gozdek, T.; Piątkowska, A. Low-Temperature Plasma Modification of Carbon Nanofillers for Improved Performance of Advanced Rubber Composites. *Polym. Bull*. **2020**, 77, 1015-1048.
17. Ren, H.; Cunha, E.; Li, Z.; et al. Silane-Functionalized Graphene Nanoplatelets for Silicone Rubber Nanocomposites. *J. Mater. Sci.* **2022**, 57, 2683-2696.
18. Ganeshkumar, S.; Vishnu, S.; Senthilvel, K.; Prabu, B. Effect of Filler on Mechanical Properties, Diffusion Kinetics, Thermal Stability, Damping and Dielectric Properties of EPDM-AGNP Nanocomposites. *Emergent Mater*. **2025**, 8, 6203-6223.
19. Abd Razak, J.; Ahmad, S. H.; Ratnam, C. T.; Shueb, M. I.; Mahamood, M. A.; Yaakub, J.; Shamsuri, S. R.; Mohamad, N. The Effects of Covalently Treated Graphene Nanoplatelet Surface Modification on Cure Characteristics, Mechanical, Physical, and Morphological Properties of NR/EPDM Rubber Blend Nanocomposites. *Adv. Environ. Biol*. **2014**, 8, 3289-3292.
20. Yadav, S. K.; Cho, J. W. Functionalized Graphene Nanoplatelets for Enhanced Mechanical and Thermal Properties of Polyurethane Nanocomposites. *Appl. Surf. Sci*. **2013**, 266, 360-367.
21. Cui, J.; Zhao, J.; Wang, S.; Li, Y. A Comparative Study on Enhancement of Mechanical and Tribological Properties of Nitrile Rubber Composites Reinforced by Different Functionalized Graphene Sheets: Molecular Dynamics Simulations. *Polym. Compos*. **2021**,

42, 205-219.
22. Tao, W.; Zhu, X.; Luo, Y.; Wang, X. Study on the Interface Properties and Thermal Conductivity of Graphene/Silicone Rubber Composites with Structural Defects and Surface Modifications. *Mater. Sci. Eng., B* **2025**, 318, 118266.
23. Hussain, S. A.; Sharma, S.; Patel, P. R. Atomistic Approach for Predicting Mechanical Properties and Creep Behavior of Graphene Reinforced Natural Rubber Composites. *Phys. Scr.* **2023**, 98, 015714.
24. Chu, C. Y.; Vukov, R. Determination of the Structure of Butyl Rubber by NMR Spectroscopy. *Macromolecules* **1985**, 18, 1423-1430.
25. He, F.; Mensitieri, G.; Lavorgna, M.; de Luna, M. S.; Filippone, G.; Xia, H.; Esposito, R.; Scherillo, G. Tailoring Gas Permeation and Dielectric Properties of Bromobutyl Rubber–Graphene Oxide Nanocomposites by Inducing an Ordered Nanofiller Microstructure. *Compos. Part B Eng*. **2017**, 116, 361-368.
26. Lewis, C.; Buanpa, R.; Kiatkamjornwong, S. Effect of Rubber Ratio, Carbon Black Level, and Accelerator Level on Natural Rubber/Bromobutyl Rubber Blend Properties. *J. Appl. Polym. Sci.* **2003**, 90, 3059-3068.
27. Motar, M. A. Inner Tube of Al-Diwanyia Tyre Based on Natural Rubber Blends. *IBN Al-Haitham J. Pure Appl. Sci.* **2010**, 23, 272-276.
28. Rodgers, M. B.; Webb, R. N.; Weng, W. Advances in Tire Innerliner Technologies. *Rubber World* **2006**, 234, 36-41.
29. Dutta, N. K.; Tripathy, D. K. Miscibility Studies in Blends of Bromobutyl Rubber and Natural Rubber. *J. Elastomers Plast.* **1993**, 25, 158-179.
30. Le, H. H.; Hait, S.; Das, A.; Wiessner, S.; Stoeckelhuber, K. W.; Boehme, F.; Reuter, U.; Naskar, K.; Heinrich, G.; Radusch, H-J. Self-Healing Properties of Carbon Nanotube Filled Natural Rubber/Bromobutyl Rubber Blends. *Express Polym. Lett.* **2017**, 11, 230.
31. Chumnum, K.; Kalkornsurapranee, E.; Johns, J.; Sengloyluan, K.; Nakaramontri, Y. Combination of Self-Healing Butyl Rubber and Natural Rubber Composites for Improving the Stability. *Polymers* **2021**, 13, 443.
32. Bello, R. H.; Coelho, L. A.; Becker, D. Role of Chemical Functionalisation of Carbon Nanoparticles in Epoxy Matrices. *J. Compos. Mater.* **2018**, 52, 449-461.
33. Causin, V.; Marega, C.; Marigo, A.; Ferrara, G.; Ferraro, A. Morphological and Structural Characterization of Polypropylene/Conductive Graphite Nanocomposites. *Eur. Polym. J.* **2006**, 42, 3153-3161.
34. Cunha, E.; Ren, H.; Lin, F.; Kinloch, I. A.; Sun, Q.; Fan, Z.; Young, R. J. The Chemical Functionalization of Graphene Nanoplatelets through Solvent-Free Reaction. *RSC Adv.* **2018**, 8, 33564-33573.
35. Englert, J. M.; Dotzer, C.; Yang, G.; Schmid, M.; Papp, C.; Gottfried, J. M.; Steinrück, H.; Spiecker, E.; Hauke, F.; Hirsch, A. Covalent Bulk Functionalization of Graphene. *Nat. Chem.* **2011**, 3, 279-286.
36. Chieng, B. W.; Ibrahim, N. A.; Yunus, W. M. Z. W.; Hussein, M. Z.; Silverajah, V. S. G. Graphene Nanoplatelets as Novel Reinforcement Filler in Poly(lactic Acid)/Epoxidized Palm Oil Green Nanocomposites: Mechanical Properties. *Int. J. Mol. Sci.* **2012**, 13, 10920-10934.
37. Yasmin, A.; Luo, J. J.; Daniel, I. M. Processing of Expanded Graphite Reinforced Polymer Nanocomposites. *Compos. Sci. Technol.* **2006**, 66, 1182-1189.
38. Intapun, J.; Rungruang, T.; Suchat, S.; Cherdchim, B.; Hiziroglu, S. The Characteristics of Natural Rubber Composites with Klason Lignin as a Green Reinforcing Filler: Thermal Stability, Mechanical and Dynamical Properties. *Polymers* **2021**, 13, 1109.
39. Charles, J.; Muthusamy, S. Comparative Study of Butyl Rubber (IIR) and Bromobutyl Rubber (BIIR) Based on FTIR, Dielectric and Thermal Studies. *J. Appl. Sci. Eng. Methodol.* **2016**, 2, 206-211.
40. Keloth Paduvilan, J.; Velayudhan, P.; Amanulla, A.; Joseph Maria, H.; Saiter-Fourcin, A.; Thomas, S. Assessment of Graphene Oxide and Nanoclay Based Hybrid Filler in Chlorobutyl-Natural Rubber Blend for Advanced Gas Barrier Applications. *Nanomaterials* **2021**, 11, 1098.
41. Rooj, S.; Das, A.; Heinrich, G. Tube-Like Natural Halloysite/Fluoroelastomer Nanocomposites with Simultaneous Enhanced Mechanical, Dynamic Mechanical and Thermal Properties. *Eur. Polym. J.* **2011**, 47, 1746-1755.
42. Rybiński, P.; Janowska, G.; Jóźwiak, M.; Pająk, A. Thermal Stability and Flammability of Butadiene–Styrene Rubber Nanocomposites. *J. Therm. Anal. Calorim.* **2012**, 109, 561-571.
43. Yin, C.; Zhang, Q.; Liu, J.; Gao, Y.; Sun, Y.; Zhang, Q. Preparation and Characterization of Grafted Natural Rubber/Graphene Oxide Nanocomposites. *J. Macromol. Sci., Part B* **2019**, 58, 645-658.
44. Krishnamurthy, S.; Balakrishnan, P. Dynamic Mechanical Behavior, Solvent Resistance and Thermal Degradation of Nitrile Rubber Composites with Carbon Black–Halloysite Nanotube Hybrid Fillers. *Polym. Compos.* **2019**, 40, E1612-E1621.
45. Yaragalla, S.; Meera, A. P.; Kalarikkal, N.; Thomas, S. Chemistry Associated with Natural Rubber–Graphene Nanocomposites and Its Effect on Physical and Structural Properties. *Ind. Crops Prod.* **2015**, 74, 792-802.
46. Boonmahitthisud, A.; Song, Z. H. Effects of Carbon Black and Carbon Nanotube on Mechanical and Thermal Properties of 80NR/20SBR Composites. In *Materials Science Forum*; Trans Tech Publications Ltd., **2010**, 654, 2783-2786.
47. Tagelsir, Y.; Li, S. X.; Lv, X.; Wang, S.; Wang, S.; Osman, Z. Effect of Oxidized and Fluorinated MWCNTs on Mechanical, Thermal and Tribological Properties of Fluoroelastomer/Carbon Black/MWCNT Hybrid Nanocomposite. *Mater. Res. Express* **2018**, 5, 065318.
48. Mensah, B.; Kumar, D.; Lim, D. K.; Kim, S. G.; Jeong, B. H.; Nah, C. Preparation and Properties of Acrylonitrile–Butadiene Rubber–Graphene Nanocomposites. *J. Appl. Polym. Sci.* **2015**, 132, 42457-42468.
49. Hernández, M.; Bernal, M. M.; Verdejo, R.; Ezquerra, T. A.; López-Manchado, M. A. Overall Performance of Natural Rubber/Graphene Nanocomposites. *Compos. Sci. Technol.* **2012**, 73, 40-46.
50. Tavakoli, M.; Katbab, A. A.; Nazockdast, H. Effectiveness of Maleic Anhydride Grafted EPDM Rubber (EPDM-g-MAH) as Compatibilizer in NR/Organoclay Nanocomposites Prepared by

Melt Compounding. *J. Macromol. Sci., Part B* **2011**, 50, 1270-1284.
51. Khalil, A.; Shaikh, S. N.; Nudrat, Z. R.; Khaula, S. Cure Characteristics, Mechanical and Swelling Properties of Marble Sludge Filled EPDM Modified Chloroprene Rubber Blends. *Adv. Mater. Phys. Chem.* **2012**, 8, 1-8.
52. Valentini, L.; Bittolo Bon, S.; López-Manchado, M. A.; Verdejo, R. Synergistic Effect of Graphene Nanoplatelets and Carbon Black in Multifunctional EPDM Nanocomposites. *Compos. Sci. Technol.* **2016**, 128, 123-130.
53. Kim, J. S.; Hong, S.; Park, D. W.; Shim, S. E. Water-Borne Graphene-Derived Conductive SBR Prepared by Latex Heterocoagulation. *Macromol. Res.* **2010**, 18, 558-565.
54. Kotal, M.; Banerjee, S. S.; Bhowmick, A. K. Functionalized Graphene with Polymer as Unique Strategy in Tailoring the Properties of Bromobutyl Rubber Nanocomposites. *Polymer* **2016**, 82, 121-132.
55. Vadukumpully, S.; Paul, J.; Mahanta, N.; Valiyaveettil, S. Flexible Conductive Graphene/Poly(vinyl chloride) Composite Thin Films with High Mechanical Strength and Thermal Stability. *Carbon* **2011**, 49, 198-205.
56. Frasca, D.; Schulze, D.; Wachtendorf, V.; Huth, C.; Schartel, B. Multifunctional Multilayer Graphene/Elastomer Nanocomposites. *Eur. Polym. J.* **2015**, 71, 99-113.
57. Yadav, S. K.; Mahapatra, S. S.; Cho, J. W.; Lee, J. Y. Functionalization of Multiwalled Carbon Nanotubes with Poly(styrene-b-(ethylene-co-butylene)-b-styrene) by Click Coupling. *J. Phys. Chem. C* **2010**, 114, 11395-11400.
58. Mondal, S.; Khastgir, D. Elastomer Reinforcement by Graphene Nanoplatelets and Synergistic Improvements of Electrical and Mechanical Properties of Composites by Hybrid Nanofillers of Graphene–Carbon Black and Graphene–MWCNT. *Compos. Part A Appl. Sci. Manuf.* **2017**, 102, 154-165.
59. Ljubic, D.; Srinivasan, M.; Szoszkiewicz, R.; Javni, I.; Petrović, Z. S. Surface Modified Graphene/Single-Phase Polyurethane Elastomers with Improved Thermo-Mechanical and Dielectric Properties. *Eur. Polym. J.* **2015**, 70, 55-65.
60. Yin, B.; Wen, Y.; Jia, H.; Wang, J.; Xu, Z.; Ding, L. Synergistic Effects of Hybridization of Carbon Black and Carbon Nanotubes on the Mechanical Properties and Thermal Conductivity of a Rubber Blend System. *J. Polym. Eng.* **2017**, 37, 785-794.
61. Innes, J. R.; Young, R. J.; Papageorgiou, D. G. Graphene Nanoplatelets as a Replacement for Carbon Black in Rubber Compounds. *Polymers* **2022**, 14, 1204.
62. Choudhury, A.; Bhowmick, A. K.; Soddemann, M. Effect of Organo-Modified Clay on Accelerated Aging Resistance of Hydrogenated Nitrile Rubber Nanocomposites and Their Lifetime Prediction. *Polym. Degrad. Stab.* **2010**, 95, 2555-2562.
63. Martins, A. F.; Visconte, L. L. Y.; Schuster, R. H.; Boller, F.; Nunes, R. C. Ageing Effect on Dynamic and Mechanical Properties of NR/Cel II Nanocomposites. *Kautsch. Gummi Kunstst.* **2004**, 57, 446-451.
64. Carli, L. N.; Roncato, C. R.; Zanchet, A.; Mauler, R. S.; Giovanela, M.; Brandalise, R. N.; Crespo, J. S. Characterization of Natural Rubber Nanocomposites Filled with Organoclay as a Substitute for Silica Obtained by the Conventional Two-Roll Mill Method. *Appl. Clay Sci.* **2011**, 52, 56-61.
65. Cao, Y.; Lai, Z.; Feng, J.; Wu, P. Graphene Oxide Sheets Covalently Functionalized with Block Copolymers via Click Chemistry as Reinforcing Fillers. *J. Mater. Chem.* **2011**, 21, 9271-9278.
66. Patole, A. S.; Patole, S. P.; Kang, H.; Yoo, J. B.; Kim, T. H.; Ahn, J. H. A Facile Approach to the Fabrication of Graphene/Polystyrene Nanocomposite by in Situ Microemulsion Polymerization. *J. Colloid Interface Sci.* **2010**, 350, 530-537.
67. Mahapatra, S. S.; Yadav, S. K.; Yoo, H. J.; Cho, J. W. Highly Stretchable, Transparent and Scalable Elastomers with Tunable Dielectric Permittivity. *J. Mater. Chem.* **2011**, 21, 7686-7691.

Publisher's Note The Polymer Society of Korea remains neutral with regard to jurisdictional claims in published articles and institutional affiliations.